Title
Epitaxially Aligned Cuprous Oxide Nanowires for All-Oxide, Single-Wire Solar Cells

Journal
Nano Letters, 14(8)

ISSN
1530-6984

Authors
Brittman, Sarah
Yoo, Youngdong
Dasgupta, Neil P
et al.

Publication Date
2014-08-13

DOI
10.1021/nl501750h

Peer reviewed

Epitaxially Aligned Cuprous Oxide Nanowires for All-Oxide, Single-Wire Solar Cells

*Sarah Brittman,[1,2]† Youngdong Yoo,[1]† Neil P. Dasgupta,[1,3] Si-in Kim,[4] Bongsoo Kim,[4] and Peidong Yang[1,2]**

† These authors contributed equally to this work.

[1]Department of Chemistry, University of California, Berkeley, California 94720, United States. [2]Materials Science Division, Lawrence Berkeley National Laboratory, 1 Cyclotron Road, Berkeley, California 94720, United States. [3]Department of Mechanical Engineering, University of Michigan, Ann Arbor, Michigan 48109, United States. [4]Department of Chemistry, KAIST, Daejeon 305-701, Korea.

* Please address correspondence to p_yang@berkeley.edu.

As a *p*-type semiconducting oxide that can absorb visible light, cuprous oxide (Cu_2O) is an attractive material for solar energy conversion. This work introduces a high-temperature, vapor-phase synthesis that produces faceted Cu_2O nanowires that grow epitaxially along the surface of a lattice-matched, single-crystal MgO substrate. Individual wires were then fabricated into single-wire, all-oxide diodes and solar cells using low-temperature atomic layer deposition (ALD) of TiO_2 and ZnO films to form the heterojunction. The performance of devices made from pristine Cu_2O wires and chlorine-exposed Cu_2O wires was investigated under one-sun and laser illumination. These faceted wires allow the fabrication of well-controlled heterojunctions that can be used to investigate the interfacial properties of all-oxide solar cells.

Keywords: copper oxide, nanowire, solar cell, photovoltaics, epitaxy, heterojunction

The optical and electronic properties of cuprous oxide (Cu_2O) make it an interesting material both for fundamental investigations and applied studies. With a direct band gap of 2.1 eV at room temperature[1] and an exciton binding energy of ~150 meV,[2, 3] Cu_2O is of interest for studying excitonic behavior as well as for solar energy conversion. It is particularly attractive for photovoltaics[4-7] and photoelectrochemistry[8-10] because it is an inexpensive, non-toxic, and earth-abundant oxide that absorbs visible light. The intrinsic *p*-type conductivity of Cu_2O arises from copper vacancies,[11, 12] and it has proven notoriously difficult to dope *n*-type.[12, 13] A variety of techniques have been used to produce Cu_2O thin films of varying quality, with the most common being high-temperature oxidation of copper metal,[7] electrodeposition,[9] and reactive sputtering.[5] Recently, many solution-phase syntheses have been developed to produce Cu_2O nanostructures with the aim of better understanding the properties of Cu_2O in single-crystalline nanocrystals[14-17] or nanowires.[18, 19]

In contrast to solution-based approaches that produce Cu_2O at low temperatures, the vapor-phase synthesis described in this work produces faceted nanowires under high-temperature conditions more similar to those used to produce the Cu_2O in the best-performing solar cells.[4, 7] These wires can then serve as a platform for studies of both the surface science and opto-electronic properties of Cu_2O and its applications, for example in photovoltaics. To this end, single-wire, all-oxide diodes and solar cells were fabricated from Cu_2O nano- and microwires by creating a $Cu_2O/TiO_2/ZnO$ heterojunction. Variation in the photocurrent and photovoltage produced by pristine Cu_2O wires and those exposed to chlorine during their synthesis suggested that the devices' performance was highly sensitive to the synthetic preparation of the wires.

Epitaxial Cu_2O nanowires were synthesized by a simple vapor transport method using a slug of copper as a precursor in an Ar/O_2 environment (Supporting Information). The Cu_2O wires grew horizontally in a single direction along the surface of the MgO (110) substrate (Figure 1a). Parallel nanowires grew over most the substrate's area. The basal width and length of the faceted nanowires

were about 500-800 nm and 10 μm, respectively (Figure 1b). Seed crystals possessing an orientation identical to that of the nanowires were observed on the same substrate (Figure 1b, inset).

Cross-sectional imaging with a transmission electron microscope (TEM) was used to characterize the crystal structure and growth direction of the nanowires. Using a gallium focused ion beam, a nanowire was cut along the plane perpendicular to its long axis and imaged using TEM (Figure 1c). The zone axis was aligned perpendicular to the surface of the cross-sectional specimen and was therefore parallel to the growth direction of the nanowire. The cross-section of the nanowires grown on MgO (110) is an isosceles triangle, and the angle between the substrate and the nanowire's side facets is 35°, which agrees well with the angle between a (110) plane and the {111} planes in Cu_2O's cubic structure (35.26°). High-resolution TEM (HRTEM) images and their fast Fourier transform (FFT) patterns confirm that the single-crystalline nanowire has {111} side facets and a (110) bottom plane, and it grows along the <110> direction with the epitaxial relationship of (110) Cu_2O // (110) MgO (Figure 1d).[20] The lattice spacing of the Cu_2O (100) planes is measured to be 0.425 nm, consistent with the expected spacing for cubic Cu_2O.

The cubic crystal structure of Cu_2O determines the morphology of the nanowires. For a cubic structure, growth along a <110> direction allows the nanowires to be enclosed by the energetically most stable {111} side facets.[14] Growth in other directions is expected to lead to the formation of less favorable facets. Because the orientations of Cu_2O and MgO have the relationship of <110> Cu_2O // <110> MgO (Figure 1d), the wires grow unidirectionally along the only available <110> direction of the MgO (110) substrate. A schematic of the atomic planes at the epitaxial interface between Cu_2O and MgO shows that the lattice mismatch between Cu_2O (110) and MgO (110) is less than 1% (Figure 1e).

When MgO (100) is used as a substrate instead of MgO (110), Cu_2O nanowires grow in two perpendicular directions (Figures 2a,b), consistent with the 4-fold symmetry of MgO (100). The cross-section of a nanowire (Figure 2c) shows that the nanowires grown on MgO (100) are the same as those on MgO (110): they have {111} side facets, a (110) bottom plane, and a <110> growth direction. X-ray

diffraction (XRD) (Figure 2d) confirms that the epitaxial relationship between the nanowires and substrate is (110) Cu_2O // (100) MgO, which is illustrated schematically (Figure 2e).

Seed crystals and shorter nanowires found throughout the substrate (Figures 2f-i) suggest that the wires nucleate as small, faceted crystals and elongate during the growth reaction. In such seed-initiated growth,[21,22] clusters of Cu_2O arriving at the substrate from the vapor migrate and nucleate to form small seed crystals on the substrate. These seed crystals have an equilibrium shape and alignment determined by the surface energy of the crystal facets and the interface energy between the crystal and the substrate.[23] Cu_2O clusters are continuously supplied to the seed crystal, leading to the horizontal nanowire growth,[21] which is energetically favorable because of the less than 1% lattice mismatch between Cu_2O and the substrate. In contrast, growth of the seed crystal in two dimensions would produce a film with a large (110) top plane, which is energetically less favorable than a wire enclosed by the more stable {111} side facets.[24]

The electrical conductivity of the nanowires was measured using a four-point contacting geometry to remove the effects of series resistance at the contacts (Figure 3). Photolithography and sputtering of ~60 nm of platinum metal was used to fabricate the devices directly on the insulating MgO substrate, and no surface pre-treatment or post-annealing was necessary to achieve ohmic contacts. Cu_2O is well known to be *p*-type, and conductivities of the wires ranged from 0.19 to 0.57 mS (Table S1). Assuming a hole mobility of 100 cm^2/Vs, based on the literature value for high-quality bulk Cu_2O films,[4, 7] the carrier concentration is estimated to be $\sim 2 \times 10^{-13}$ cm^{-3} derived from the conductivity and geometry of the wires. Given the large size of these wires, it is not expected that their surface would significantly reduce their carrier mobility. The conductivity and estimated carrier concentration are consistent with those found in high-quality Cu_2O thin films used in the record planar solar cells.[4, 7] The wires also exhibited photoconductivity under simulated solar illumination (Figure 3).

Fabrication of the heterojunction solar cells was a multistep process applied to the MgO substrate (Supporting Information). Briefly, after contacting one end of the wire with platinum, O_2 etching of poly(methyl methacrylate) (PMMA) was used to pattern the region that would become the

heterojunction. The substrates then underwent low-temperature atomic layer deposition of either ZnO (~30 nm) or amorphous TiO_2 (~10-20 nm) and then ZnO. Such depositions were performed well below the glass temperature of PMMA (~120°C) to avoid damaging the lithographic patterning or excessively annealing the oxide interface. Deposition of ZnO was performed at 85°C in contrast to typical deposition temperatures that usually exceed 100°C.[25] After deposition of the films, the PMMA was lifted off and the ZnO contacted with titanium and gold, yielding the finished devices (Figures 4a-b).

The heterojunction devices typically functioned as diodes, especially when the TiO_2 interlayer was included to avoid interfacial chemistry between the Cu_2O and diethylzinc used to deposit ZnO. Most devices, however, did not exhibit photocurrent or photovoltage under one-sun illumination, and their *I-V* characteristics show significant hysteresis, which might have arisen from the charging and discharging of trap states at the interface (Figure 4c). Under more intense illumination, provided by a HeCd laser at λ=442 nm, the devices did produce photocurrent and a photovoltage (Figure 5a). Because the doping of the heterojunction is highly asymmetric, with a carrier concentration of ~6×10^{18} cm^{-3} in the ZnO deposited at 85°C (Table S2) but only ~10^{13} cm^{-3} in Cu_2O, a large depletion width is expected within the Cu_2O wire, which could prevent efficient collection of majority carriers through the depleted Cu_2O. Scanning photocurrent mapping (SPCM) of these devices shows that the photocurrent is localized to the edge of the core-shell region (Figure 5b), which is consistent with this explanation.

In an effort to improve the conductivity of the Cu_2O wires, chlorine, which is a known extrinsic *p*-type dopant for Cu_2O,[12, 26, 27] was introduced into reactions via the in-situ decomposition of $MgCl_2$[26] (Supporting Information). In all samples, XRD confirmed that the wires were Cu_2O (Figure S1), and four-point resistivity measurements indicated marginal increases in conductivity (Table S1).

Some devices produced from these chlorine-exposed wires exhibited a clear photoresponse under one-sun conditions, and their performance was evaluated quantitatively. Efficiencies were calculated based on the cross-sectional area of the devices as measured by SEM (Table S3), with the champion device reaching 0.38% (Figure 6a). For comparison, the record planar Cu_2O/ZnO solar cell achieved an efficiency of 4.12%.[4] Scanning photocurrent mapping (SPCM) of the wire devices showed, however,

that only parts of the core-shell region were active, which partly accounts for their low photocurrent (Figure S2). FF's below the theoretical limit of 0.25 (Table S3) arose from the inverse curvature of some of the *I-V* curves in the fourth quadrant, suggesting severe recombination at the heterojunction and indicating a need for improved understanding of the interface. Wavelength-dependent photocurrent measurements showed an abrupt decrease in photocurrent at approximately 600 nm, which corresponds to the band gap absorption of Cu_2O (588 nm) given that the full-width, half-maximum of the monochromatic excitation was approximately 15 nm (Figure 6b). The low V_{oc}'s and FF's are reminiscent of Cu/Cu_2O Schottky junctions,[26] perhaps produced by oxidation-reduction chemistry at the wire's surface. Alternatively, since a reduced shunt resistance from the metal contacts is unlikely based on the geometry of the device, either there is a light-activated shunt resistance across the interface itself, or the photocurrent collection within the Cu_2O is assisted by the electric field rather than mediated by diffusion to the junction.[28] This second explanation is consistent with the expectation that the Cu_2O core of the wires is nearly fully depleted, so assuming that the carriers have a low drift mobility-lifetime product ($\mu\tau$), the efficiency of charge collection could depend upon the strength of the electric field within the Cu_2O, which is reduced under applied forward bias.

All devices exhibiting photocurrent and photovoltage under one-sun conditions (one-sun devices) were produced from Cu_2O wires grown in the presence of chlorine, although not all chips of such wires produced one-sun devices. Because these devices were clustered on particular chips rather than spread across all samples and multiple chips underwent the lithographic and ALD processing in parallel, it is likely that the performance of the devices was dictated by a characteristic of the Cu_2O wires that was uniform across a given chip but not controllable between different chips. Some possibilities for this critical characteristic include (1) the bulk doping concentration of the wires, (2) the surface coverage of the wires in chlorine, or (3) the exposed crystallographic facets of the wires. Chlorine was originally introduced into the reaction to reduce the asymmetry in carrier concentration of the Cu_2O/ZnO junction and improve charge collection through the Cu_2O core. If the incorporation of chlorine into the wires varied, perhaps only some chips contained wires that were sufficiently doped to allow charge collection

and therefore measurable photocurrents and photovoltages under one-sun conditions. Studies on II-VI quantum dots indicate that halides are excellent ligands for passivation of surface states on II-VI materials such as PbS.[29] Since the performance of the Cu_2O/ZnO heterojunction is known to be highly sensitive to the chemistry of the interface,[4] the chloride surface treatment could reduce the interfacial states of the heterojunction and therefore improve its ability to separate photogenerated charges. Lastly, SEM images indicate that exposure to the chlorine gas during the growth can alter the exposed crystal facets of the wires (Figure S2). Many (but not all) of the devices that demonstrated one-sun photocurrent and photovoltage exhibited {100} side facets rather than the {111} side facets found in pristine Cu_2O wires (Figure S2). As the surface chemistry of Cu_2O is known to depend on the exposed crystallographic facet,[15, 24] it is possible that the oxidation-reduction chemistry or the crystallographic orientation of the interface with ZnO varied with different crystal facets of the Cu_2O. Given the complexity of the chlorine-exposed growth and the fabrication processes of the Cu_2O wires, further systematic investigation is required to determine the reason for the photovoltaic performance of the devices fabricated from chlorine-exposed wires.

Beginning with Cu_2O wires synthesized in a vapor-phase reaction at high temperature, single-wire ZnO/Cu_2O and ZnO/TiO_2/Cu_2O heterostructure diodes were fabricated. Devices showed photocurrent and photovoltage under laser illumination, and some devices produced from wires exposed to chlorine during their growth showed photovoltaic performance under one-sun illumination. Possible explanations for the difference in performance between the pristine and chlorine-exposed wires include bulk doping of the Cu_2O wire to improve its charge collection or differences in the heterojunction's interfacial chemistry such as passivation with surface chlorine atoms or the varying oxidation-reduction potential of different crystal facets of Cu_2O. These wires offer a platform for future investigation of these effects not only in the Cu_2O/ZnO heterojunction but also in heterojunctions between Cu_2O and more promising oxides, such as gallium oxide (Ga_2O_3), which has produced the current record 5.38%-efficient Cu_2O solar cell.[4] If combined with techniques that can provide improved control over the deposition of the *n*-type oxide, such as room-temperature pulsed laser deposition,[4, 7] these wires have the potential to offer

detailed insight into the structural and electrical performance of the heterojunction in Cu_2O-based solar cells.

Acknowledgement

Funding from the National Science Foundation Center of Integrated Nanomechanical Systems (NSF COINS) under contract No. 0832819 is greatly appreciated. Y.Y. acknowledges a postdoctoral fellowship from the NRF of Korea under Basic Science Research Program funded by the MEST (2012R1A6A3A03039763). N.P.D. acknowledges support from the U.S. Department of Energy through an Office of Energy Efficiency and Renewable Energy (EERE) Postdoctoral Research Award under the SunShot Solar Energy Technologies Program.

Supporting Information Available

Conductivities of the pristine and chlorine-exposed wires. Conductivities and Hall-effect measurements of ZnO films deposited by low-temperature ALD. XRD and facet identification of the chlorine-exposed wires. Photovoltaic performance and SPCM of solar cells made from chlorine-exposed wires.

Figure Captions

Figure 1. Cu_2O nanowires grown epitaxially in a single direction on a MgO (110) substrate. (a-b) Top-view SEM images of the nanowires and a seed crystal (c) Cross-sectional TEM image of a nanowire obtained by cutting the wire with a focused-ion beam. (d) HRTEM image and FFT patterns of the square in (c) indicating the epitaxial relationship between Cu_2O and MgO. (e) Schematic showing the lattice arrangement at the interface between the nanowire and the substrate.

Figure 2. Cu_2O nanowires grown epitaxially in two perpendicular directions on a MgO (100) substrate. (a-b) Top-view and (c) cross-sectional SEM images of the nanowires. (d) XRD pattern of the nanowires on a MgO substrate, indicating that they are Cu_2O grown epitaxially on the substrate. (e) Schematic showing the lattice arrangement at the interface between the nanowire and the substrate. (f-i) Top-view

SEM images of the nanocrystals formed at different locations on the same substrate, suggesting that the wires nucleate as seed crystals and then elongate during the growth process.

Figure 3. Conductivity of a Cu_2O wire. Four-point conductivity and photoconductivity under one-sun illumination of a wire grown without chlorine. Inset: SEM image of a four-point device.

Figure 4. Characterization of single-wire devices made from pristine Cu_2O wires. (a-b) SEM images of a $Cu_2O/TiO_2/ZnO$ device showing the wire blanketed by the thin films. (c) A typical *I-V* curve of a device in the dark and under solar illumination. While the devices did show evidence of photoconductivity, they did not exhibit a photovoltage or photocurrent without more intense illumination. Devices also showed hysteresis, with more current produced during the backward scan (down from higher to low voltage) than during the forward scan.

Figure 5. Response of the devices to laser illumination. (a) Devices exhibited photocurrent and photovoltage under HeCd laser illumination (λ=442 nm), with both increasing with the light's intensity. Curves correspond to order-of-magnitude increases in the illumination's intensity. (b) SPCM of a device under HeCd illumination showing that the current decays rapidly from the edge of the device's core-shell region into the core-shell region, suggesting that photogenerated carriers created far from this interface cannot be collected. (c) Optical reflection image acquired simultaneously with the photocurrent map in (b). Red corresponds to the most reflective surfaces (e.g. the metal electrode), while yellow indicates scattering or absorption (e.g. the wire and edges of the electrode or the ZnO film). Maps are approximately 12 × 6 μm.

Figure 6. Characterization of the solar cells produced from chlorine-exposed Cu_2O wires. (a) *I-V* curve in the dark and under one-sun illumination of the most efficient single-wire device. (b) Normalized

photocurrent as a function of wavelength, indicating that the spectral response of the devices is consistent with the absorption of Cu_2O.

References

1. Nakano, Y.; Saeki, S.; Morikawa, T. *Appl. Phys. Lett.* **2009,** 94, (2), 022111.
2. Kavoulakis, G. M.; Chang, Y.-C.; Baym, G. *Phys. Rev. B* **2007,** 55, (12), 7593-7599.
3. O'Hara, K. E.; Wolfe, J. P. *Phys. Rev. B* **2000,** 62, (19), 12909-12922.
4. Nishi, Y.; Miyata, T.; Minami, T. *Thin Solid Films* **2013,** 528, 72-76.
5. Lee, Y. S.; Heo, J.; Winkler, M. T.; Siah, S. C.; Kim, S. B.; Gordon, R. G.; Buonassisi, T. *J. Mater. Chem. A* **2013,** 1, (48), 15416.
6. Musselman, K. P.; Marin, A.; Schmidt-Mende, L.; MacManus-Driscoll, J. L. *Adv. Funct. Mater.* **2012,** 22, 2202-2208.
7. Minami, T.; Nishi, Y.; Miyata, T. *Appl. Phys. Exp.* **2013,** 6, (4), 044101.
8. Paracchino, A.; Laporte, V.; Sivula, K.; Gratzel, M.; Thimsen, E. *Nature Mater.* **2011,** 10, (6), 456-61.
9. Paracchino, A.; Brauer, J. C.; Moser, J.-E.; Thimsen, E.; Graetzel, M. *J. Phys. Chem. C* **2012,** 116, (13), 7341-7350.
10. Paracchino, A.; Mathews, N.; Hisatomi, T.; Stefik, M.; Tilley, S. D.; Grätzel, M. *Energy Environ. Sci.* **2012,** 5, (9), 8673.
11. Raebiger, H.; Lany, S.; Zunger, A. *Phys. Rev. B* **2007,** 76, 045209.
12. Biccari, F. Defects and Doping in Cu_2O. Sapienza-University of Rome, Rome, 2009.
13. Scanlon, D. O.; Watson, G. W. *J. Phys. Chem. Lett.* **2010,** 1, 2582-2585.
14. Sui, Y.; Fu, W.; Yang, H.; Zeng, Y.; Zhang, Y.; Zhao, Q.; Li, Y.; Zhou, X.; Leng, Y.; Li, M.; Zou, G. *Cryst. Growth Des.* **2010,** 10, (1), 99-108.
15. Hua, Q.; Cao, T.; Bao, H.; Jiang, Z.; Huang, W. *ChemSusChem* **2013,** 6, 1966-1972.
16. Zhang, Y.; Deng, B.; Zhang, T.; Gao, D.; Xu, A.-W. *J. Phys. Chem. C* **2010,** 114, 5073-5079.
17. Susman, M. D.; Feldman, Y.; Vaskevich, A.; Rubinstein, I. *ACS Nano* **2014,** 8, (1), 162-174.
18. Tan, Y.; Xue, X.; Peng, Q.; Zhao, H.; Wang, T.; Li, Y. *Nano Lett.* **2007,** 7, (12), 3723-3728.
19. Hacialioglu, S.; Meng, F.; Jin, S. *Chem. Commun.* **2012,** 48, (8), 1174-6.
20. Markworth, P. R.; Chang, R. P. H.; Sun, Y.; Wong, G. K.; Ketterson, J. B. *J. Mater. Res.* **2001,** 16, (4), 914-921.
21. Yoo, Y.; Seo, K.; Han, S.; Varadwaj, K. S. K.; Kim, H. Y.; Ryu, J. H.; Lee, H. M.; Ahn, J. P.; Ihee, H.; Kim, B. *Nano Lett.* **2010,** 10, (2), 432-438.
22. Yoo, Y.; Yoon, I.; Lee, H.; Ahn, J.; Ahn, J.-P.; Kim, B. *ACS Nano* **2010,** 4, (5), 2919-2927.
23. Silly, F.; Castell, M. R. *Phys. Rev. Lett.* **2005,** 94, (4), 046103.
24. Zheng, Z.; Huang, B.; Wang, Z.; Guo, M.; Qin, X.; Zhang, X.; Wang, P.; Dai, Y. *J. Phys. Chem. C* **2009,** 113, 14448-14453.
25. Guziewicz, E.; Kowalik, I. A.; Godlewski, M.; Kopalko, K.; Osinniy, V.; Wójcik, A.; Yatsunenko, S.; Łusakowska, E.; Paszkowicz, W.; Guziewicz, M. *J. Appl. Phys.* **2008,** 103, (3), 033515.
26. Olsen, L. C.; Addis, F. W.; Miller, W. *Solar Cells* **1982,** 7, 247-279.
27. Biccari, F.; Malerba, C.; Mittiga, A. *Sol. Energy Mater. Sol. Cells* **2010,** 94, (11), 1947-1952.
28. Mazhari, B. *Sol. Energy Mater. Sol. Cells* **2006,** 90, (7-8), 1021-1033.
29. Ning, Z.; Ren, Y.; Hoogland, S.; Voznyy, O.; Levina, L.; Stadler, P.; Lan, X.; Zhitomirsky, D.; Sargent, E. H. *Adv. Mater.* **2012,** 24, (47), 6295-9.

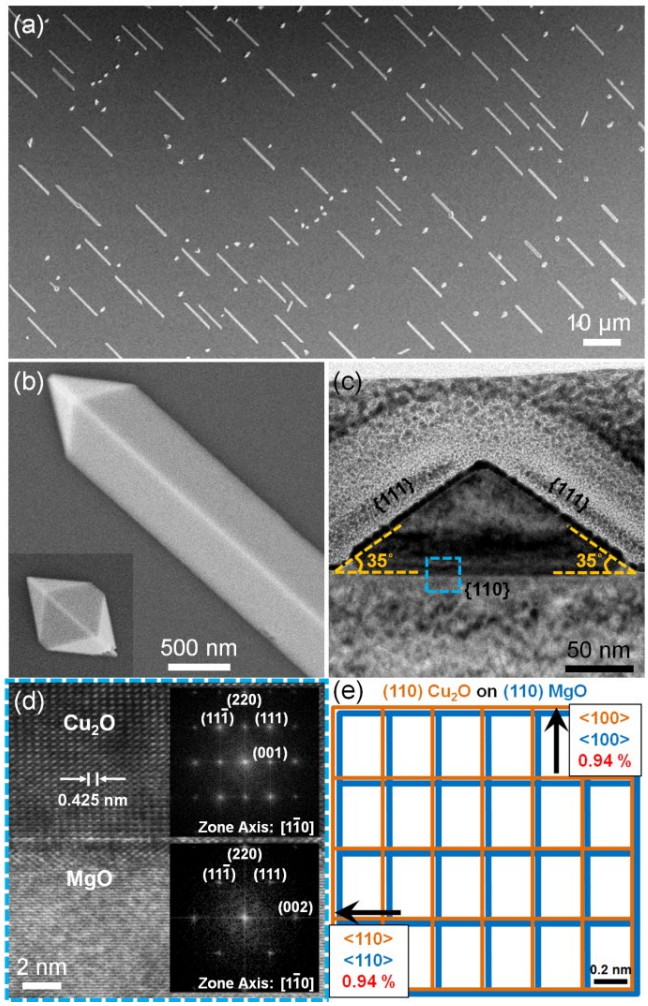

Figure 1

Figure 2

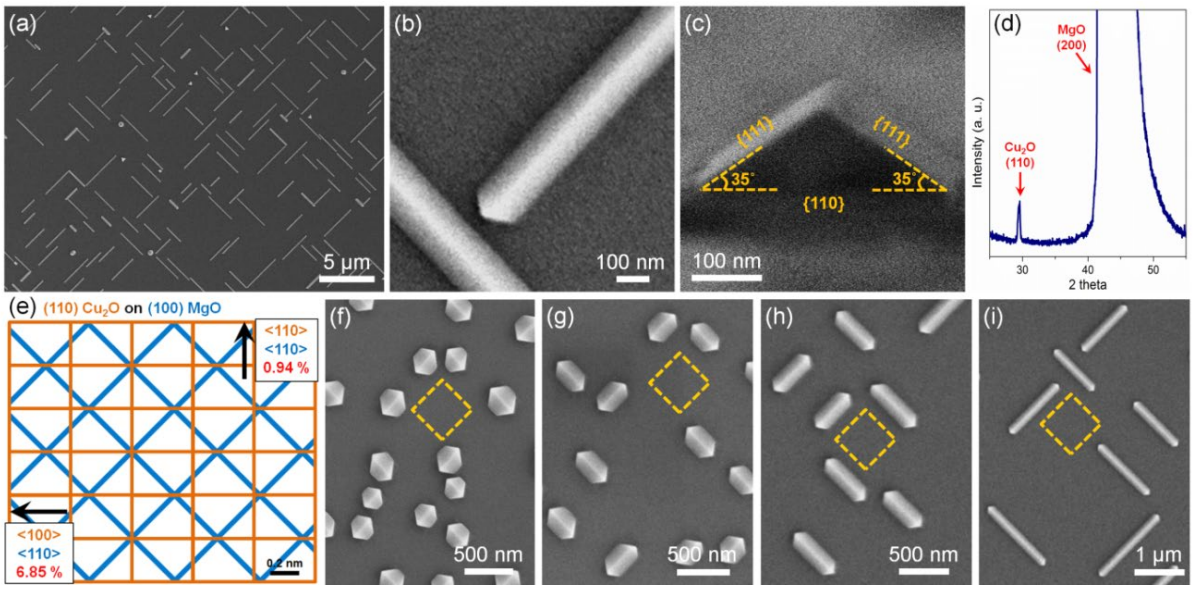

Figure 3

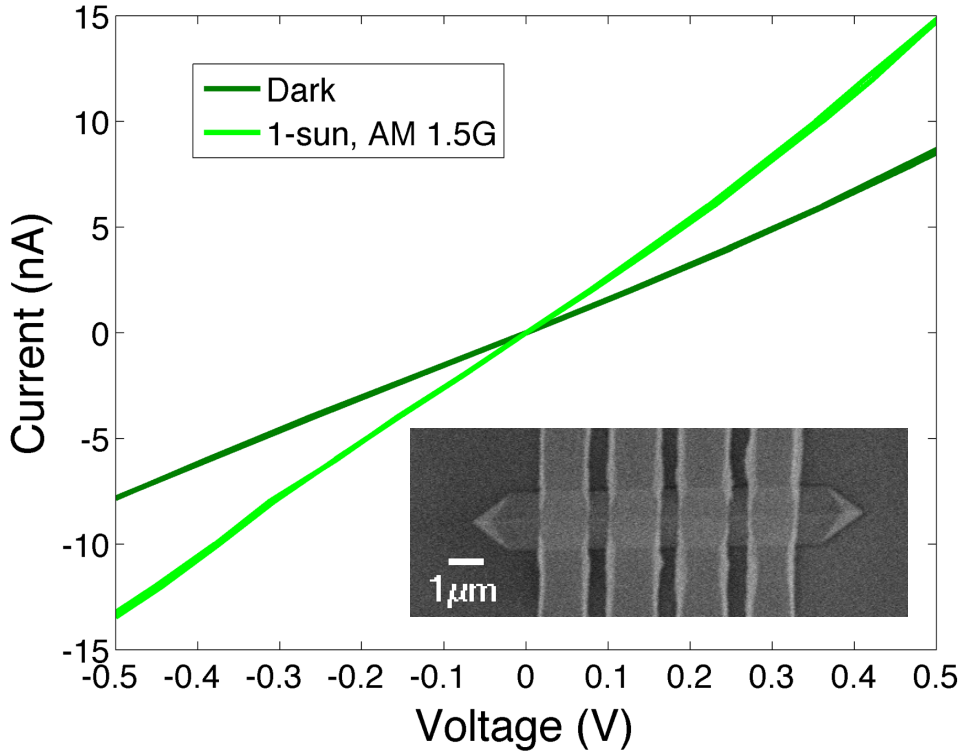

Figure 4

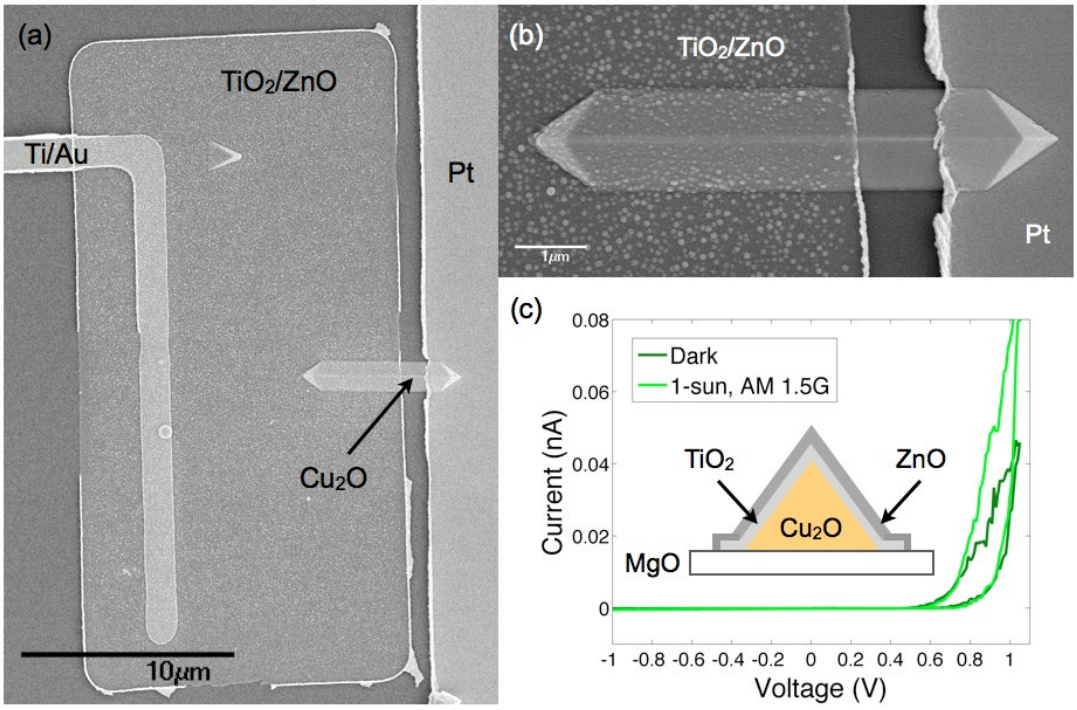

Figure 5

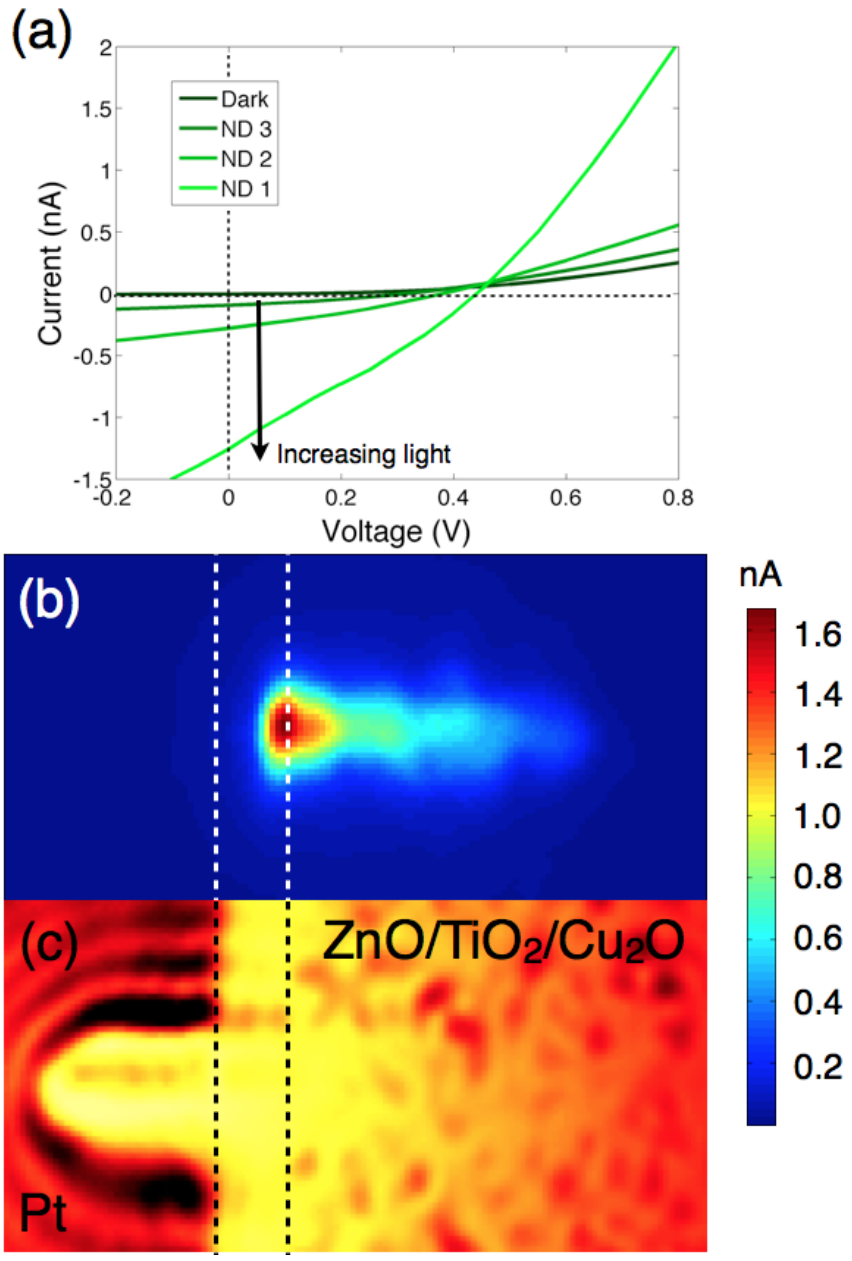
(a)
Dark
ND 3
ND 2
ND 1
Current (nA)
Increasing light
Voltage (V)
(b)
(c)
ZnO/TiO2/Cu2O
Pt
nA
1.6
1.4
1.2
1.0
0.8
0.6
0.4
0.2

Figure 6

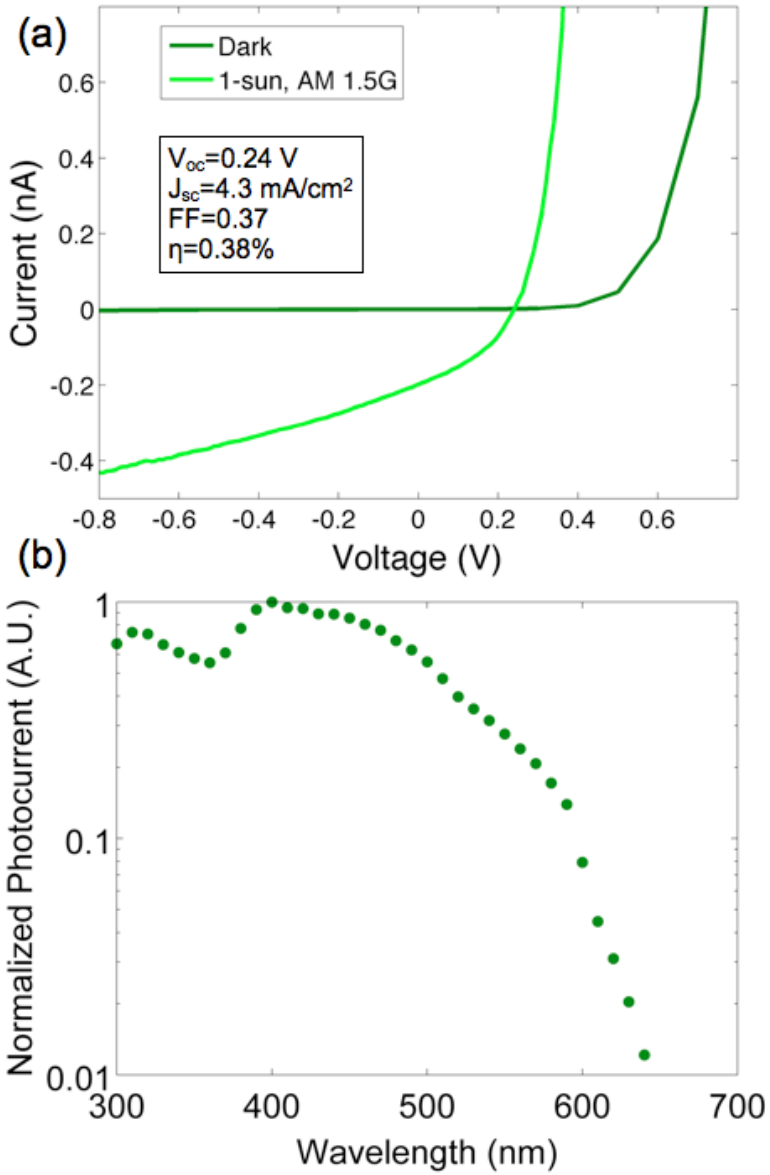
(a)
Dark
1-sun, AM 1.5G
V_{oc}=0.24 V
J_{sc}=4.3 mA/cm²
FF=0.37
η=0.38%
Current (nA)
Voltage (V)
(b)
Normalized Photocurrent (A.U.)
Wavelength (nm)